Complexes Formed between Calmodulin and the Antagonists J-8 and TFP in Solution†

C. Jeremy Craven,‡ Brian Whitehead,‡ Sheena K. A. Jones,‡ Eva Thulin,§ G. Michael Blackburn,|| and Jonathan P. Waltho*,‡

Department of Molecular Biology and Biotechnology and Department of Chemistry, Krebs Institute, University of Sheffield, P.O. Box 594, Sheffield S10 2UH, U.K., and Department of Physical Chemistry 2, Chemical Centre, University of Lund, Lund, Sweden

Received February 29, 1996; Revised Manuscript Received May 20, 1996⊗

ABSTRACT: The binding of the antagonists *N*-(8-aminooctyl)-5-iodonaphthalene-1-sulfonamide (J-8) and trifluoperazine (TFP) to intact calcium-saturated bovine calmodulin (CaM) and also of J-8 to the C-terminal domain (tr2c) has been investigated. Using a combination of NMR methods, including NOESY data, mobility measurements, and chemical shift and line-shape analysis, we show that the primary interaction between J-8 and tr2c is between the naphthalene ring of the antagonist and the hydrophobic pocket of the protein, similar to the binding of the hydrophobic side-chain residues of calmodulin target peptides. Comparison of the mobility of the drug, the intensity and pattern of intermolecular NOESY cross-peaks, and chemical shift changes shows that there is no significant change in the binding mode in J-8·CaM compared to J-8·tr2c, with one molecule binding to each domain. In particular, we find that the mobility of the aliphatic amino "tail" of J-8 remains highly mobile in both systems. This contrasts with the notion that the tail may bridge between the two domains to give a "globular" form of CaM. We also show that TFP induces very similar shift changes to J-8 and that the stoichiometry of the major binding event in all three cases is one drug molecule per domain. It also appears that secondary binding sites for the drug molecules are present in all three systems.

Calmodulin (CaM)[1] plays a central role as the primary transducer of calcium-dependent signals in eukaryotes and as a regulator of essential cellular function (Andersson & Malencik, 1986; Rasmussen *et al*., 1992; Finn & Forsén, 1995). In response to increased intracellular calcium levels it binds with high affinity to a wide range of target proteins involved in, for example, cyclic nucleotide and glycogen metabolism, NADP synthesis, calcium translocation, contractility, and motility (Hait & Lazo, 1986). CaM is composed of two domains linked together by a flexible tether (Barbato *et al*., 1992), the individual domains of intact CaM having mobility approaching that expected for the cleaved domains in isolation. The cleaved, isolated domains, termed tr1c and tr2c for the N- and C-terminal domains, respectively, when combined produce a solution NMR spectrum very similar to that of intact CaM, indicating the relatively independent nature of the domains in the intact protein (Dalgarno *et al*., 1984a). Indeed, the solution structure of tr2c (Finn *et al*., 1995) matches very closely that of the C-terminal domain of intact CaM as determined by both X-ray crystallography and NMR spectroscopy (Babu *et al*., 1985; Ikura *et al*., 1992; Meador *et al*., 1992, 1993).

The regions of the target proteins with which CaM interacts consist of sequences of primarily basic and hydrophobic residues (O'Neil & DeGrado, 1990). The complexes formed between CaM and peptides corresponding to these regions have high affinity, and a number of their structures have been determined at high resolution, namely, the complexes formed with a 26-residue peptide (named M13) from skeletal muscle myosin light chain kinase (skMLCK; Ikura *et al*., 1992), a 20-residue peptide from smooth muscle myosin light chain kinase (smMLCK; Meador *et al*., 1992), and a 25-residue peptide from brain CaM-dependent protein kinase II (CaMKII; Meador *et al*., 1993). In each complex, the peptides are predominantly helical and are "clamped" by the N- and C-terminal domains, each of which provides a hydrophobic surface to interact with hydrophobic residues toward the two ends and on opposite faces of the peptide. The conformation of the individual CaM domains is not significantly perturbed by peptide binding. The global structure of the molecule, however, changes from that of a "dumbbell" consisting of two effectively independent domains to a much more compact "globular" form. In each domain the hydrophobic surface contains a pocket that accommodates either a large hydrophobic side chain, *e.g*.,

† We acknowledge financial support from the Yorkshire Cancer Research Campaign (S.K.A.J.), BBSRC (C.J.C.), SmithKline Beecham (B.W.), the British Council, and the EU COST Programme and acknowledge use of the BBSRC 600 MHz NMR Instrument in Edinburgh. The Krebs Institute is a BBSRC Biomolecular Science Centre for Molecular Recognition.

* Corresponding author.

‡ Department of Molecular Biology and Biotechnology, University of Sheffield.

§ University of Lund.

|| Department of Chemistry, University of Sheffield.

⊗ Abstract published in *Advance ACS Abstracts,* July 15, 1996.

[1] Abbreviations: COSY, correlation spectroscopy; CaM, calmodulin; CaMKII, calmodulin-dependent protein kinase II; HSQC, heteronuclear single-quantum coherence spectroscopy; HMQC, heteronuclear multiple-quantum coherence spectroscopy; J-8, *N*-(8-aminooctyl)-5-iodonaphthalene-1-sulfonamide; M13, 26-residue peptide from skMLCK; NMR, nuclear magnetic resonance; NOE, nuclear Overhauser effect; NOESY, nuclear Overhauser effect spectroscopy; smMLCK, smooth muscle myosin light chain kinase; skMLCK, skeletal muscle myosin light chain kinase; TFP, trifluoperazine; TOCSY, total correlation spectroscopy; tr1c, N-terminal domain of CaM (residues 1−75); tr2c, C-terminal domain of CaM (residues 76−148).

S0006-2960(96)00504-1 CCC: $12.00 © 1996 American Chemical Society

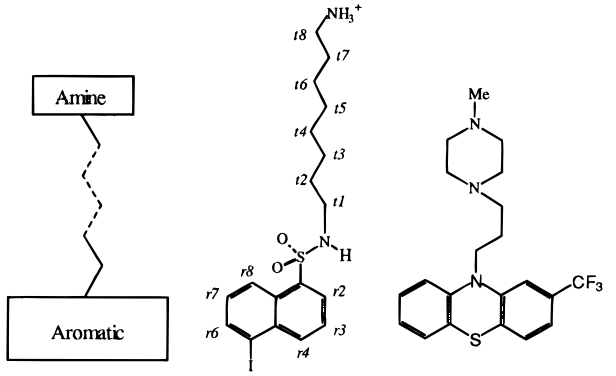

FIGURE 1: (a) Schematic representation of the paradigm for CaM binding drugs introduced by Prozialeck and Weiss (1982). (b and c) Chemical structures of J-8 and TFP. The observable resonances in J-8 are labeled. The sulfonamide and amine protons exchange rapidly with the solvent in aqueous solution, and their resonances are not observed.

tryptophan, or a combination of side chains, *e.g.*, leucine and isoleucine. The importance of these pockets in the geometry of binding of the peptides is reflected in the interdomain movement observed for the CaM complex with CaMKII compared with those for smMLCK and skMLCK (Meador *et al.*, 1993). In the former complex, the N- and C-terminal domains move closer together, in which positions of the hydrophobic residues in this sequence (separated by one turn less of the peptide helix) are accommodated in the hydrophobic pockets.

As a result of the involvement of CaM in the control of a range of metabolic processes, much interest has developed in CaM agonists and antagonists. For example, CaM is found at elevated levels in several tumor cell lines (Wei *et al.*, 1981, 1982; Hickie *et al.*, 1983), and CaM antagonists have been shown to reduce tumor size *in vivo* (MacNeil *et al.*, 1988). Numerous pharmacological agents currently in clinical use, as well as a range of small, hydrophobic molecules, have been shown to inhibit CaM-dependent processes. Such drugs range from antidepressants, *e.g.*, nimodipine, through antimalarial agents, *e.g.*, quinacrine, to anesthetics, *e.g.*, lidocaine (Hait & Lazo, 1986). Apart from the hydophobicity and the generally basic nature of these molecules, little is understood about their binding to CaM or their mode of inhibition of CaM-dependent activation. There is some controversy over measurements of their binding affinities (which have been reported up to 3 orders of magnitude different depending on the method of measurement; Lopes *et al.*, 1990) and in particular the stoichiometry of binding of these small molecules to CaM (Andersson *et al.*, 1985).

In this work, we study the interactions between bovine CaM and the two antagonists J-8 and trifluoperazine (Figure 1). J-8 (MacNeil *et al.*, 1988) is an analogue of *N*-(6-aminohexyl)-5-chloro-1-naphthalenesulfonamide (W-7) that shows a high degree of selectivity for the inhibition of CaM-dependent versus CaM-independent calcium-stimulated processes. Trifluoperazine (TFP) is a phenothiazine family antipsychotic drug.

The structures of J-8 and TFP conform to a paradigm for CaM binding drugs introduced by Prozialeck and Weiss (1982). Such drugs have two main features in common: a hydrophobic aromatic "head" with a basic "tail" attached via an aliphatic side chain. Two X-ray structures (Vandonselaar *et al.*, 1994; Cook *et al.*, 1994) have been reported for CaM complexes with TFP. These two structures, which are the first experimental CaM−drug complexes to be determined, partially address the roles of the head and tail of the drug but raise other questions concerning the binding of such drugs. One of the structures (Cook *et al.*) contains one molecule of TFP per CaM molecule, whereas the other (Vandonselaar *et al.*) contains at least four molecules. The differences were ascribed to different ratios of TFP·CaM used in crystallization solutions (4.5:1 *versus* 35:1). However, Cook *et al.* still observed only one molecule of TFP per CaM at an increased ratio of 11.5:1. The observed crystal structure is clearly sensitive to the crystallization conditions. Despite these differences, a striking feature common to both of these studies is the compact globular conformation adopted by CaM on binding the drug molecule(s). The form of the complex with a hydrophobic tunnel resulting from the juxtaposition of the hydrophobic patches of the N- and C-terminal domains of CaM is very similar to that seen in the peptide complexes. There are, however, fundamental differences between the two published structures, concerning the interactions between the TFP molecules and the two domains. The single TFP molecule in the Cook structure predominantly interacts with the hydrophobic pocket in the C-terminal domain. In this structure, the sole close contacts to the N-terminal domain are between the CF_3 group and Glu11. In the Vandonselaar structure, TFP molecules bind into the hydrophobic pockets of each domain but with the phenothiazine moiety reversed, inserting the CF_3 group into the hydrophobic pockets. In this structure the interaction between the TFP that binds into the C-terminal domain and the N-terminal domain is a proposed electrostatic interaction between Glu11 and the piperazine ring of the TFP molecule.

The aim of the present work is to investigate whether, in solution, the binding of antagonists to CaM is inherently a process involving both domains or whether a good antagonist could bind effectively independently to each or either domain. Our strategy is to first characterize the binding of an antagonist to one domain (tr2c) and then compare this with the binding to the two-domain protein. This is the only way in which the autonomy of the domains can be conclusively established.

In addition to having structural features typical of other CaM binding drugs, J-8 has two properties which simplify NMR spectroscopy. The majority of the protons in the naphthalene ring resonate in the amide proton region of the protein; thus ^{15}N filtering allows the ring protons to be studied free from overlap with protein resonances. Also, the two nitrogen atoms cause dispersion of the methylene resonances in the tail, allowing most of the tail resonances to be assigned. For these reasons it has been possible to obtain more detailed information about the J-8 systems than about the binding of TFP.

We have used four NMR probes to characterize the binding of the drugs to tr2c and CaM, namely, chemical shift changes on binding, drug mobility measurements, exchange broadening effects, and NOEs. The chemical shift changes can be used to compare the binding of the two different drugs to the one- and two-domain proteins, even though it appears that the magnitudes and directions of the changes cannot be simply interpreted. COSY spectra of J-8 complexed with tr2c and CaM allow us to compare the mobility of various

parts of the drug molecule in the two complexes. The study of exchange broadening allows us to examine in detail the stoichiometry of drug binding in all three systems. Finally, intermolecular NOEs in the J-8•tr2c and J-8•CaM complexes allow us to locate more precisely the site of drug binding and also to gain additional information about the dynamics of the drug within the binding site.

EXPERIMENTAL PROCEDURES

Sample Preparation. *N*-(8-Aminooctyl)-5-iodonaphthalene-1-sulfonamide (J-8) was prepared from 5-amino-1-naphthalenesulfonic acid and 1,8-diaminooctane (purchased from Fluka Chemicals) using the method described previously (MacNeil *et al*., 1988) and recrystallized from ethanol. The purity of J-8 was greater than 99.5% as determined using ^{1}H NMR. TFP was purchased as the dihydrochloride salt (minimum 99% purity) from Sigma. Unlabeled and uniformly ^{15}N-labeled recombinant bovine tr2c and CaM were prepared as described previously (Andersson *et al*., 1983; Vogel *et al*., 1983). Purified, lyophilized calcium-free protein was dissolved to a concentration of 4 mM (tr2c) or 1.5 mM (CaM) in H_2O containing 10% D_2O and 0.02% NaN_3, and appropriate quantities of $CaCl_2$ solution were added to yield calcium-saturated protein. Calcium saturation was checked by observing diagnostic amide shifts in the 1D spectrum. The final sample volume was 500 μL. The pH of the solutions was adjusted to 6.0 using dilute HCl and NaOH. Stock solutions of the drugs were prepared at a concentration of 33 mM in CD_3OD for J-8 or 30 mM in D_2O for TFP. The pH of the protein solutions was monitored throughout the titrations, and where necessary small additions of acid or base were made to maintain the pH at 6.0.

NMR Spectroscopy. All NMR experiments were carried out on a Bruker AMX 500 spectrometer operating at a proton resonance frequency of 500 MHz or a Varian Unity 600 operating at 600 MHz. The H_2O resonance was suppressed by on-resonance low power presaturation (typically applying a 50 Hz field for 800 ms) during the relaxation delay, followed by a SCUBA sequence (Brown *et al*., 1988) employing two composite Π pulses separated by 30 ms delays. For homonuclear two-dimensional spectra, 128 signal-averaged transients were collected over acquisition times of 48 × 328 ms. For heteronuclear two-dimensional spectra, 8 or 16 signal-averaged transients were collected over acquisition times of 50 × 328 ms. For three-dimensional spectra, 8 signal-averaged transients were collected over acquisition times of 41 × 23 × 41 ms. ^{15}N/^{1}H HSQC (Bodenhausen & Ruben, 1980), double-quantum-filtered COSY (Rance *et al*., 1983), two-dimensional NOESY (mixing times: 75, 150, 200 ms; Macura *et al*., 1981) and three-dimensional ^{1}H/^{15}N TOCSY-HMQC (spin-lock period: 70 ms), and NOESY-HMQC (mixing times: 75 and 150 ms; Marion *et al*., 1989a) experiments were recorded using standard pulse sequences, modified by the inclusion of a spin-echo prior to acquisition or with premature activation of the receiver prior to chemical shift or *J* coupling refocusing, as described previously (Waltho & Cavanagh, 1993). The ω_2-half-filtered NOESY spectra (Otting *et al*., 1986) were acquired with a 150 ms mixing time at 311 K and acquired such that both ^{15}N-selected and ^{15}N-excluded spectra could be obtained for direct comparison between drug−protein and protein−protein cross-peaks for checking cross-peak assignments. Acquisition times were 36 × 328 ms. The mixing time was chosen to maximize sensitivity, while accepting that there would be a small amount of spin diffusion present. The rather loose constraint bounds used should ensure that the structure calculations are not adversely affected by this. For the 1:1 J-8•tr2c and 2:1 J-8•CaM spectra two duplicate experiments were run to improve sensitivity, giving a total number of transients per increment of 384 and 320, respectively. For the 1:1.6 J-8•tr2c spectrum, 192 transients were acquired. The acquired data were processed using the program FELIX (Biosym Technologies Inc.) running on Silicon Graphics workstations. Prior to transformation a low-frequency deconvolution filter was applied to the acquisition dimension to remove the residual water signal (Marion *et al*., 1989b). Typically a phase-shifted sine-bell window function was applied prior to Fourier transformation. Proton and nitrogen frequencies were referenced relative to TSP [3-(trimethylsilyl)[2,2,3,3-$^2H_4$]propionate], using a value of 0.101329118 for γ_N/γ_H (Wishart *et al*., 1995).

tr2c and CaM Assignment. The ^{1}H and ^{15}N backbone and side-chain resonances of tr2c were assigned at both 301 K and 311 K, pH 6.0 (data available from the authors upon request), using standard methods. For J-8•tr2c, the amide ^{1}H/^{15}N correlations were followed in the titration series of HSQC spectra (see Results), using three-dimensional TOCSY-HMQC and NOESY-HMQC and two-dimensional COSY experiments to resolve ambiguities and identify side-chain resonances at the end point of the titration. The assignment is essentially complete, apart from residues M76 and K77, for which no ^{1}H/^{15}N correlations could be observed, and residues D78, E82, E84, and E87, which could neither be followed unambiguously in the HSQC titration nor be reassigned in the 1:1 solution due to the lack of unambiguous sequential NOEs. In the solution structure of calcium-loaded tr2c, the first helix is well structured from approximately residue 83 onward (Finn *et al*., 1995). The methyl groups of the methionine residues were not fully assigned due to the lack of unambiguous NOEs. By comparison with tr2c and with the assignment for *Drosophila* calmodulin of Ikura *et al*. (1990), a substantial number of ^{1}H/^{15}N correlations in the HSQC spectra of CaM could be assigned and then followed in the titration series for both J-8 and TFP.

J-8 Assignment. The assignment of J-8 in the absence of tr2c was carried out using methanol as the solvent, as the drug has relatively low water solubility. The proton spectrum of J-8 has six resolved aromatic resonances, which were divided into two three-proton spin systems via COSY connectivities. The pair of resonances corresponding to the protons *r2* and *r8* were identified from the observation of cross-peaks to the side-chain resonances in a NOESY spectrum of the drug−protein complex. Distinguishing *between* these two resonances (and hence the other four resonances) was not trivial due to the high degree of symmetry of the molecule. A long-range carbon−proton correlation experiment did not yield useful information, because of the similar values for the medium- and long-range couplings in the naphthalene ring. The assignment was therefore completed by using characteristic chemical shifts of the proton and carbon resonances in comparison to the model compounds 1-naphthalenesulfonic acid and 1-iodonaphthalene. The proton spectrum of each of these compounds was readily assigned as in each case the molecule divides into a three- and a four-proton system. The carbon

and proton shifts observed in these molecules provide strong evidence that the most downfield-shifted doublet (8.66 ppm) in J-8 corresponds to *r8*; this identification allowed the assignment of all six ring protons to be completed. The methylene protons, which lie at opposite ends of the drug side chain, resonate at very similar frequencies (2.83 and 2.84 ppm, respectively). The assignment of these two resonances was based on the observation of a correlation between *t1* and the amide proton of the sulfonamide group in the COSY spectrum. This sulfonamide resonance is observed only in methanol solution, and not in aqueous solution, due to solvent exchange. The remainder of the methylene assignments were completed using COSY connectivities based on the assignments of *t1* and *t8*. In the J-8·tr2c complex the changes in chemical shift of J-8 were sufficiently small that the transfer of the assignment from the free solution was straightforward.

Line-Shape Analysis. Line shapes were calculated for a simple two-state exchange model using the equations of McConnell (1958), as expressed in Sandström (1982). The transverse relaxation times were adjusted to match the observed line width, and the value of the off-rate was varied to optimize the agreement between the calculated and experimental data. A normalizing factor was applied to all data to correct for the constant intensity loss observed throughout the titration as a result of dilution and possibly some precipitation of bound protein. This was calculated by determining the mean intensity loss of a number of peaks for which no change in chemical shift was seen on binding J-8 and hence were unaffected by the exchange processes.

In interpreting the line-shape analysis in terms of absolute stoichiometry, it is imperative that one can be certain of the drug and protein concentrations used. For the protein this was initially determined by UV absorbance and for the drug by dry weight. The final concentrations in the 2:1 complexes were then checked by comparison of peaks in 1D spectra which confirmed that the concentrations were correct to within approximately 10%.

Chemical Shift Calculations. Proton chemical shifts were calculated using the program *total* written by Dr. M. P. Williamson, which implements the model parameterized by Williamson and Asakura (1993). This model includes terms for ring current C═O and C′−N bond anisotropy, and electric field effects.

Structure Calculations. Constraints were obtained from cross-peaks in the ^{15}N-filtered NOESY spectrum. When a NOESY cross-peak could be potentially identified (by a match of frequencies) as being between side-chain and ring protons of the drug, this identification was assumed, and such cross-peaks were excluded from the calculations. The only constraints included in the calculations, therefore, were between the naphthalene ring protons of the drug and the protein. The chemical shift values of the peak centers were converted to "ambiguous" X-PLOR constraint lists (Nilges, 1995) using our own software. The input for this procedure consisted of the complete resonance assignment of the protein, the positions of the aromatic resonances of J-8, and the list of cross-peak centers. A tolerance of 0.03 ppm was used for matching peak centers to the assignments [this was the middle value used by Nilges (1995)]. This assignment procedure was implemented as a simple *awk* program. All constraints were given an upper bound of 5 Å. This relatively conservative choice was made because of the difficulty of faithfully converting cross-peak intensities to more precise distances when there is the possibility of multiple binding and ill-defined dynamics. Fixed protein coordinates taken from the 1.7 Å resolution X-ray structure of vertebrate calmodulin (Chattopadhyaya *et al*., 1992; PDB entry 1CLL) were used in the calculations. The rationale for using fixed coordinates was that comparison of this structure with the 2 Å resolution structure of calmodulin complexed with the calmodulin binding domain of calmodulin-dependent protein kinase II (Meador *et al*., 1993; PDB entry 1CDM) reveals that the changes in the structure of the individual domains of calmodulin on peptide binding are extremely small. A fresh J-8 starting conformation for each calculation was created by first transforming the coordinates in an extended conformation by a random rigid body rotation. The center of mass was then placed, at random, within a box of side 60 Å centered on the center of mass of the protein molecule. The J-8 molecule was then treated as flexible, subject to constraints of covalent geometry and van der Waals contacts. Structures were calculated with X-PLOR 3.1 (Brünger, 1992), using a molecular dynamics simulated annealing protocol similar to those used for conventional protein structure determination (Nilges *et al*., 1988a,b). For the first 3 ps, a high temperature (1500 K) was maintained, and the weight on the core repulsion potential energy term was kept very low. This was followed by a 18 ps cooling stage (Brünger, 1992) in which the temperature was reduced in 50 K steps, and the weight on the core repulsion term was gradually increased. Finally, the structures were subjected to 250 steps of conjugate gradient energy minimization. As a refinement stage, the temperature was increased to 1500 K and the above cycle repeated. During the high-temperature stage of the protocol, a square-well NOE potential was used, with harmonic sides. During the second part of the protocol, the X-PLOR *soft-square* potential was used, which smoothly changes the harmonic potential to a linear potential for large constraint violations. The energy constant for the harmonic potential was 5.0 kcal mol^{-1} Å^{-2}. The slope of the asymptote was 0.5 kcal mol^{-1} Å^{-1}. The switching region between the two regimes was approximately between 0.5 and 2 Å above the upper constraint bound. The *parallhdg.pro* parameter set of X-PLOR was used, with the X-PLOR quartic *repel* potential to represent the repulsive part of the interatomic interactions. No attractive or electrostatic terms were used. The final weight on the repulsive term was 4 kcal mol^{-1} Å^{-4}.

For the analysis of constraints, we defined the NOE-equivalent distance as follows. Suppose a constraint has M possible assignments according to the assignment list and suppose that it is desired to analyze a set of N structures. Denoting the distance represented by the ith assignment in the jth structure as d_{ij}, then the NOE-equivalent distance, r_{NOE}, for a constraint is

$$r_{NOE} = \left(\frac{1}{N}\sum_{j=1}^{N} D_j^{-6}\right)^{-1/6}$$

where

$$D_j = \left(\sum_{i=1}^{M} d_{ij}^{-6}\right)^{-1/6}$$

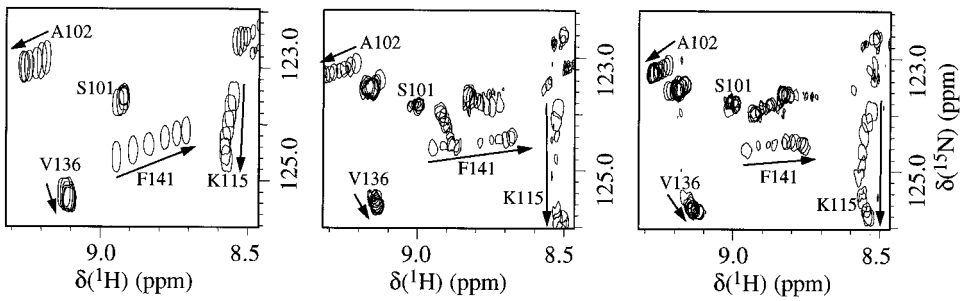

FIGURE 2: Region of the HSQC titration series for the three systems studied, showing an overlay of spectra up to a final concentration of drug of 1 equiv per domain. From left to right: (a) J-8•tr2c; (b) J-8•CaM; (c) TFP•CaM. Only peaks in the C-terminal domain are labeled. The arrows show the dirction of movement of the peaks with increasing drug concentration. Only a single contour level is plotted for each peak.

In constructing random data sets, it was important to maintain both the symmetry of the spectrum and the correlations between peaks involving adjacent ring protons (which are necessarily close in space). This was achieved by randomizing the resonance assignment rather than the peak positions. In order to ensure that the degree of ambiguity was also retained, the randomization was achieved by simply scrambling the correspondence between the list of parts per million values and the list of resonance names. This ensured that each peak was assigned with the same number of possibilities as for the original experimental data set but to a random set of resonances. Different random data sets were constructed by using a different seed for the random number generator in the scrambling process.

RESULTS

Titrations and Resonance Assignment. For all systems studied (J-8 with tr2c, J-8 with CaM, and TFP with CaM), the drug was titrated in aliquots of 0.2 protein equiv into a uniformly ^{15}N-labeled sample of the protein. After the addition of each aliquot of drug, 1D ^{1}H and 2D ^{1}H/^{15}N HSQC spectra were acquired. The J-8/tr2c titration was performed up to a maximum J-8:tr2c molar ratio of 1.6:1, while the J-8/CaM and TFP/CaM titrations were performed up to maximum drug:protein molar ratios of 2:1 and 4:1, respectively. Regions of the ^{1}H/^{15}N HSQC spectra of tr2c in the titration series are shown overlaid in Figure 2a. Panels b and c of Figure 2 show this same area for CaM in the J-8 and TFP titrations, respectively. This figure demonstrates that, in contrast to the binding of peptides derived from target proteins to CaM, the binding of both drugs is in the fast exchange regime; i.e., the resonances move gradually as more drug is added. This is consistent with the measured binding constant for J-8 ($\sim$10 μM, unpublished results) and a diffusion controlled on-rate (Creighton, 1984). A table of the shift changes induced in tr2c on binding J-8 is available as Supporting Information.

Figure 3a is a plot of the amide ^{1}H and ^{15}N chemical shift changes for the C-terminal domain residues which could be assigned in all three systems, namely (from left to right), tr2c upon J-8 binding, CaM upon J-8 binding, and CaM upon TFP binding. This figure shows the course of the titration up to a concentration of drug of 1 equiv/domain.

Analysis of the behavior of the different resonances in the titrations in detail reveals a variety of different phenomena. For tr2c at drug concentrations up to 1:1 the movement of most resonances was linear; however, some of the traces were distinctly curved, especially those of T110 and M145. Above the 1:1 point, distinct curvature was apparent for several more of the traces (Figure 3b). The direction and magnitude of the shifts in CaM/J-8 and in CaM/TFP were very similar to those in the J-8/tr2c titration. Particularly striking was F92, which disappeared immediately on the addition of the first aliquot of drug in all three cases and only reappeared at a drug concentration of approximately 0.7 equiv/domain. For J-8 some small differences were observed between the behavior of full CaM and the single domain, particularly in the last two C-terminal residues and those close to the central helix, the latter presumably due to truncation effects. In addition, K115 shifted somewhat further in CaM than in tr2c, in both the J-8 and TFP titrations. Distinct curvatures were again observed for several residues in both the CaM titrations. Titrating a further 2 equiv of TFP into CaM caused three different types of chemical shift changes, representative examples of which are shown in Figure 3c. Most of the residues which showed large shift changes during the addition of the first two drug equivalents were hardly affected by the next two equivalents, as seen for K115. A few residues, however, continued to shift either in the same direction (*e.g.*, I130) or in a different direction (*e.g.*, N111).

Less assignments were made for residues in the N-terminal domain of CaM; however, shifts of a range of magnitudes similar to those seen in the C-terminal domain were observed for both J-8 and TFP binding. Also, resonances in both domains moved simultaneously as drug was added, demonstrating that the drug binds with approximately equal affinity to both domains.

Many authors have stressed the importance of interactions between methionine methyl groups and various molecules binding into the hydrophobic pocket of calmodulin (Finn & Forsèn, 1995; Reid *et al.*, 1990). Although the five methionine methyl groups in tr2c were not fully assigned, the very sharp singlets from the methyl protons were easily observed in the one-dimensional spectrum of the free protein. The most downfield-shifted resonance was relatively unaffected by J-8 binding, showing only a very slight upfield shift. This signal was also absent from the spectrum of the thrombin fragment of CaM (Dalgarno *et al.*, 1984b), which consisted of residues 107−148, and was thus assigned as M76. One of the methionine peaks could be followed in the one-dimensional titration, showing a relatively large chemical shift change of 0.24 ppm. The other three resonances disappeared with the addition of $<$0.2 molar equiv of J-8 and could not be relocated at later stages of the titration. These resonances must therefore be substantially shifted, and a value of $>$0.2 ppm was assumed when

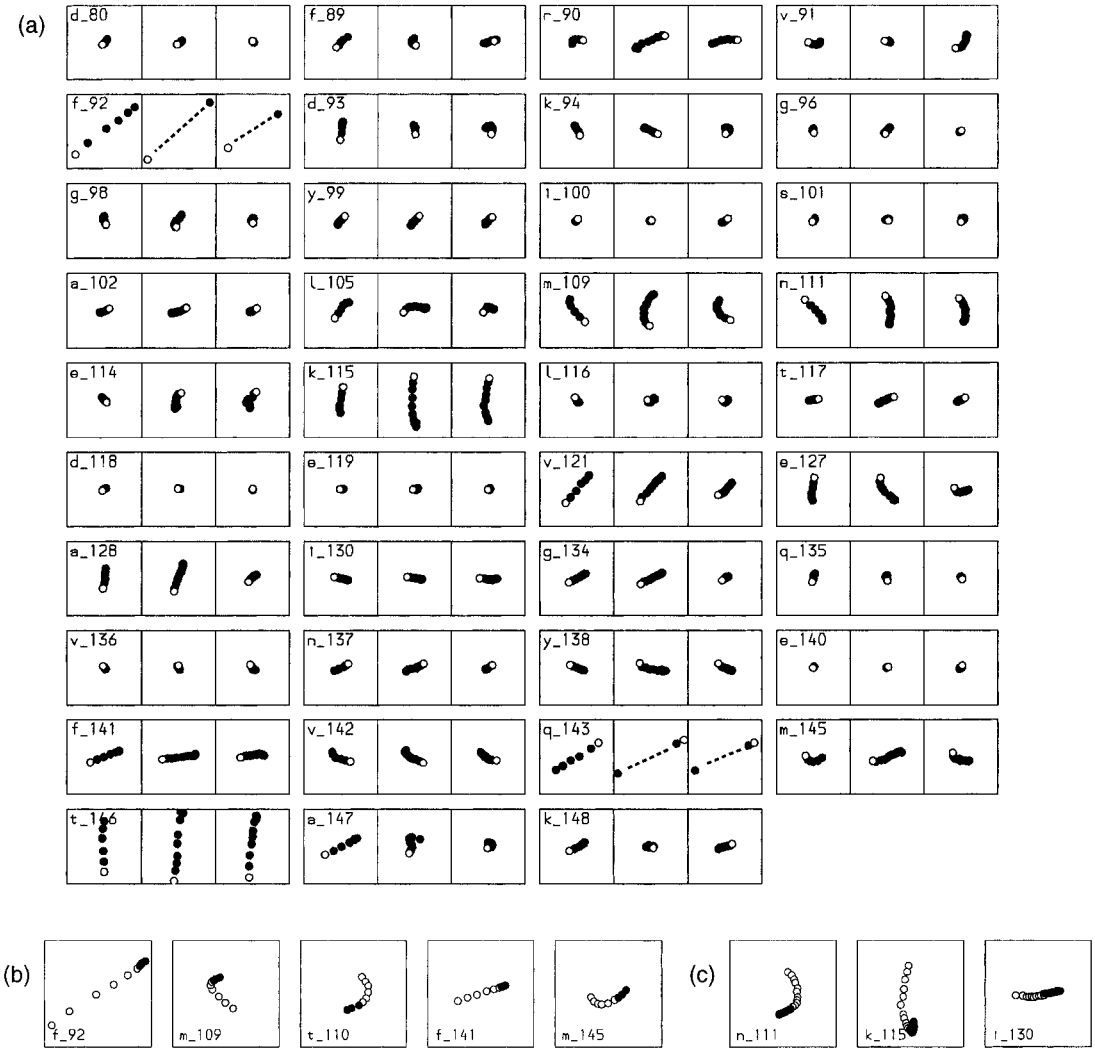

FIGURE 3: Movement of the $^1H/^{15}N$ correlation peaks in the HSQC titration series. The figures were made by first extracting the ^1H and ^{15}N chemical shifts for each resonance at each point in the titration. These shifts are then plotted against each other individually for each resonance shown. Each box represents a region of 300 × 200 Hz, with the ^1H shift plotted horizontally and the ^{15}N shift plotted vertically. (a) C-Terminal residues for which the resonances could be assigned in all three systems; plotted from left to right for each residue are J-8•tr2c, J-8:CaM, and TFP•CaM. The first point in each titration is shown as an open symbol. (b) Examples from the J-8•tr2c titration continued up to a concentration of 1.6:1. (c) Examples from the TFP•CaM titration continues up to a concentration of 4:1. In (b) and (c) the second part of the titration is shown as filled circles. For F92 the peak could only be located at the beginning and end points of the titration due to line broadening. Similarly, for Q143 only the first two points in the titration could be followed, further points being severely broadened and the end point falling in a crowded region of the spectrum.

compiling the side-chain shift changes. Six sharp resonances could be observed for the nine methionines in CaM; again the most downfield resonance remained sharp throughout the drug titrations, whereas the others disappeared with the addition of <0.2 molar equiv of drug.

The ^1H assignments for J-8 in solution and in complex with tr2c and CaM at 311 K are given in Table 1.

Line-Width Changes. The protein resonances which show the largest chemical shift changes (of up to 300 Hz for the proton resonances at 500 MHz) experience significant exchange broadening and therefore reduction of peak height at intermediate drug concentrations. The peak heights throughout the J-8/tr2c titration of residues F92, F141, and G134 are shown in Figure 4a. An estimate for the off-rate of 3500 ± 1000 s^{-1} was obtained from these data (see Experimental Procedures), the solid curves in Figure 4a showing the corresponding calculated variation of peak height for the three residues. Most of the peaks almost fully resharpened by the end of the titration, establishing a stoichiometry of 1:1 for this binding event. In contrast, the heights of several resonances dropped steeply toward the 1:1 point, in particular, T110 and F89, and remained at low

Table 1: Chemical Shifts of J-8, in Solution and Complexed with tr2c and CaM

		complexed with tr2c[b]		complexed with CaM[b]	
resonance	free[a] δ	δ	$\Delta\delta$	δ	$\Delta\delta$
r2	8.42	8.15	−0.27	8.10	−0.32
r3	7.68	7.42	−0.26	7.37	−0.29
r4	8.25	8.01	−0.24	8.04	−0.21
r6	8.26	7.80	−0.46	7.92	−0.34
r7	7.39	7.21	−0.18	7.26	−0.13
r8	8.78	8.63	−0.15	8.75	−0.03
t1	2.85	2.75	−0.10	2.76	−0.09
t2	1.29	1.27	−0.02	1.32	0.03
t3,4,5[c]	1.08	1.03	−0.05	1.08	0.00
t6	1.23	1.14	−0.09	1.17	−0.06
t7	1.57	1.49	−0.08	1.54	−0.03
t8	2.85	2.85	0.00	2.88	0.03

[a] Methanol-d_4, 311 K. [b] Water, pH 6.0, 311 K. [c] Unresolved resonances.

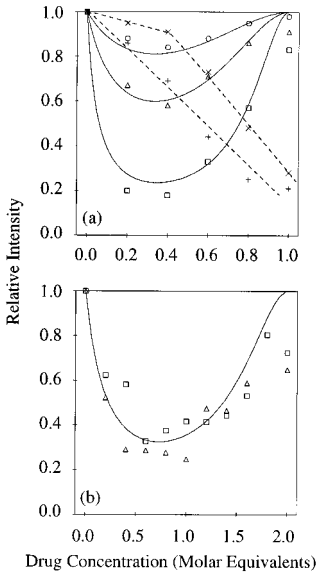

FIGURE 4: Experimental and calculated HSQC cross-peak intensities during the titration series. Panels: (a) J8·tr2c; experimental data for F92 (□), F141 (△), G143 (○), F89 (×), and T110 (+); solid lines are calculated (see text); dashed lines are drawn to guide the eye. (b) Experimental data for K115 in J8·CaM (△) and TFP·CaM (□); the solid line is calculated (see text).

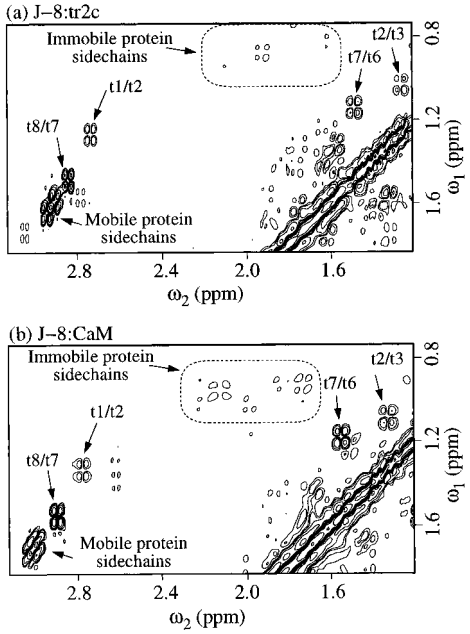

FIGURE 5: COSY spectra of (a) 1:1 J-8·tr2c and (b) 2:1 J-8·CaM. The spectra are plotted at a high contour level to show the particularly intense peaks due to highly mobile groups. Immobilized groups thus only show as very weak peaks (within boxed regions).

intensity up to the highest concentration studied. The reasons for this are discussed further below.

Similar exchange broadening effects were observed in the CaM/drug titrations. It was not possible to measure these peak intensities with the same precision, since the signal to noise ratio was worse for these spectra. Typically errors of 25% were obtained for the intensity measurements. The height changes for K115, which gives an intense cross-peak and which has a large shift change (∼100 Hz) in both titrations, are shown in Figure 4b. In both cases the height returns to near the initial value at a 2:1 drug protein ratio, establishing a 2:1 stoichiometry. The solid curve in this figure shows the height change calculated for the binding with an off-rate of 800 s^{-1}. No indications could be found for any binding events with a stoichiometry of 1:1.

COSY Spectra. Figure 5 shows a region of the 2D COSY spectra for the tr2c·J-8 and CaM·J-8 complexes which encompasses the cross-peaks for all the resolvable J-8 tail resonances. The line width and hence the intensity of the COSY peaks give direct information about the dynamics of the drug molecule. *In both tr2c·J-8 and CaM·J-8*, the COSY cross-peak at the distal end of the tail (*t7*/*t8*) is extremely intense, whereas the corresponding cross-peak at the other end of the chain (*t1*/*t2*) is much weaker. The cross-peaks corresponding to methylene groups between these two extremes show a corresponding gradation of intensity. It is possible to qualitatively characterize the mobility implied by these variations in intensity by direct comparison with protein cross-peaks. The *t1*/*t2* cross-peak intensity is similar to that of typical protein side-chain cross-peaks, whereas the *t7*/*t8* cross-peak is as sharp as that due to the highly mobile side chains of hydrated basic residues. The drug therefore appears to be tethered to the protein at the aromatic end, with the aliphatic tail retaining high mobility.

NOESY Spectra. A portion of the ^{15}N ω_2-half-filtered NOESY spectrum (Otting *et al*., 1986) of a solution of a 1:1 molar ratio of J-8·tr2c at 311 K, pH 6.0, is shown in Figure 6. As five of the six aromatic proton resonances of J-8 lie within a region of the spectrum that contains only nitrogen-bound proton resonances of tr2c, the filtering allows differentiation between drug and protein resonances in ω_2. The only protein resonances in this region of the filtered spectrum in ω_2 are the aromatic resonances of Phe92 and His107. The positions of the J-8 resonances are marked on the figure. In the absence of such filtering, it was impossible to confidently discern any drug−protein peaks, due to the coincidence of J-8 and protein resonances.

The most intense cross-peaks at the J-8 aromatic proton frequencies appear to arise from NOEs within the drug molecule, to the proximal protons (*t1*−*5*) of the drug tail. This interpretation is supported by the fact that the pattern of the intensities of these cross-peaks is consistent with purely *intra*molecular distances. For instance, strong cross-peaks are observed between ring resonances *r2* and *r8* and the first methylene group (*t1*) of the side chain, weaker cross-peaks are observed to the next two methylene resonances (*t2* and the unresolved resonances of *t3*, *t4*, and *t5*), and no cross-peaks are observed to the final three methylene groups (*t6*, *t7*, and *t8*). The cross-peaks from the other ring resonances are correspondingly weaker. The pattern of aromatic−aromatic cross-peaks within the drug is also consistent with purely intramolecular distances. The intradrug NOEs observed between ring protons are strong and negative, implying a correlation time similar to that of most of the protein side chains. In contrast, the *t7*/*t8* cross-peak is positive, indicating a high degree of mobility for the distal end of the tail. Again, this demonstrates mobility for the end of the J-8 tail similar to that of mobile basic side chains.

There remain, however, a number of cross-peaks that must arise from drug−protein interactions. Although the extreme weakness of these NOEs precludes a "high-resolution" structure determination of the complex, an analysis of the NOEs was made by docking a J-8 molecule to a fixed conformation of the protein, using NOE-based constraints.

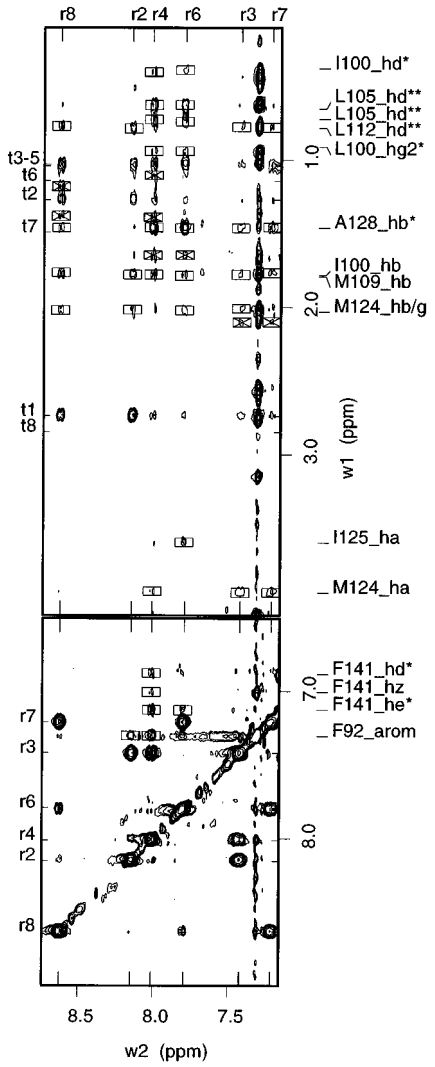

FIGURE 6: Portion of the filtered NOESY spectrum of the 1:1 J-8•tr2c solution. This spectrum is processed to *exclude* nitrogen-bound resonances in the ω_2 dimension. In the filtered dimension, only the portion of the spectrum including the drug naphthalene ring protons is shown. In the ω_1 dimension the portion of the spectrum between 4.0 and 6.7 ppm is omitted as it contains no cross-peaks. The boxes mark the cross-peaks used as constraints in the structure calculations. The boxes marked with a cross are those constraints which gave no reasonable assignment within either orientation class. The positions of J-8 resonances are marked along the left-hand and top edges of the figure. The spectrum is contoured just above the noise level, with the contours plotted logarithmically, each contour representing a change in intensity by a factor of 1.8. The chemical shifts of the resonances to which the cross-peaks were assigned are shown along the right-hand edge of the figure.

An ambiguous constraint list was constructed, using the data from 45 drug−protein cross-peaks from the NOESY spectrum. The cross-peaks used for constructing the constraint list are marked in Figure 6 with boxes; on average, each peak was 3.6-fold ambiguous, and the greatest ambiguity was 6-fold. Using this set of constraints and a dynamic assignment protocol (Nilges, 1993), 120 initial structures were calculated, as described in Experimental Procedures. A family of 50 structures with similarly low energies were then selected for further analysis. The NOE-equivalent distances for this family of structures are plotted in Figure 7 (large symbols). The majority of the constraints fall within the shaded range and are thus loosely satisfied. The distribution of distances shows a distinct kink for the final eight constraints, which we discuss below.

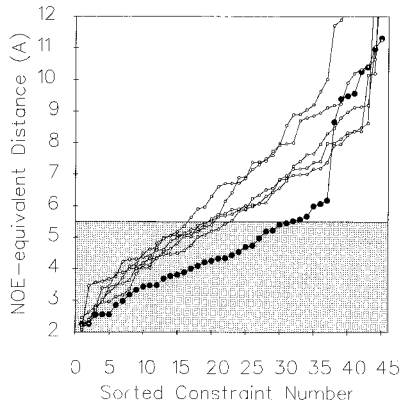

FIGURE 7: NOE-equivalent distances for the constraints calculated in the initial structure calculations, using experimental data (large symbols) or random data (small symbols). For each set of data the constraints are ordered according to distance. The shaded portion represents distance up to 0.5 Å above the 5 Å upper bound. For the definition of NOE-equivalent distance, see Experimental Procedures.

There is a strong symmetry in the occurrence of NOEs to the pairs of resonances (*r2* and *r8*), (*r3* and *r7*), and (*r4* and *r6*), which is consistent only with the ring binding into the pocket in two orientations. The two orientations differ in that the normal to the plane of the ring points in opposite directions relative to a fixed orientation of the protein. Indeed, the calculated structures could be divided into two classes containing 22 and 28 structures depending on the direction of the normal to the ring plane relative to the protein. As a final stage of refinement, the constraints were divided into two sets. The first set (31 constraints) contained constraints that gave NOE-equivalent distances of less than 6 Å in one of the orientation classes, while the second set (28 constraints) contained constraints corresponding to the second class. Constraints that satisfied both selection criteria were included in both classes. Eight constraints violated both classes (the eight cross-peaks above the kink in Figure 7 referred to above), which are probably peaks for which the method cannot find an appropriate assignment. These could be peaks whose apparent peak centers are distorted by peak overlap or noise or which arise from secondary binding events or which correspond to unassigned resonances. For instance, it must be highly likely that NOESY cross-peaks exist to the unassigned methionine methyl resonances. Using a more elaborate model, allowing an ensemble of conformers for instance, it might be possible to assign some of these cross-peaks, but we did not feel that the quantity of data available justified such further parameterization. We preferred, therefore, to simply exclude these cross-peaks from further calculations. These cross-peaks are marked by crossed boxes in Figure 6. The refinement stage of the protocol was then repeated, using the appropriate reduced set of constraints for each structure depending on its class. The changes in the mean structures following this refinement were extremely small, with a change in the rmsd overlap of the ring heavy atoms of less than 0.7 Å. This insensitivity to the removal of a number of badly violated constraints must be due to a combination of the low force constant for large constraint violations (due to the use of a small asymptotic gradient in the *soft* potential) and steric hindrance. A stereoview of the minimized average structure in one of the two distinct ring orientations is shown in Figures 8 and 9. In the second orientation (not shown) the ring is ap-

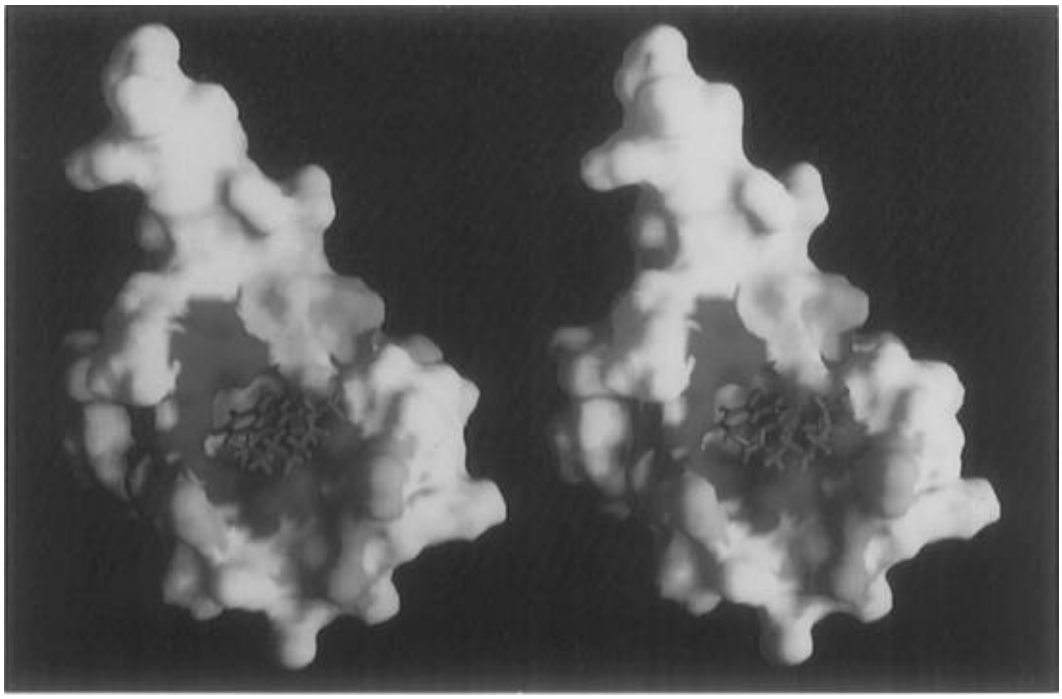

FIGURE 8: Stereo image of one of the calculated minimized average conformations of the J8·tr2c complex. The surface representation of tr2c [created using GRASP (Nicholls, 1993)] is colored according to the largest side-chain shift of each residue, with gradation from white (shifts <0.04 ppm) to dark blue (shifts >0.23 ppm).

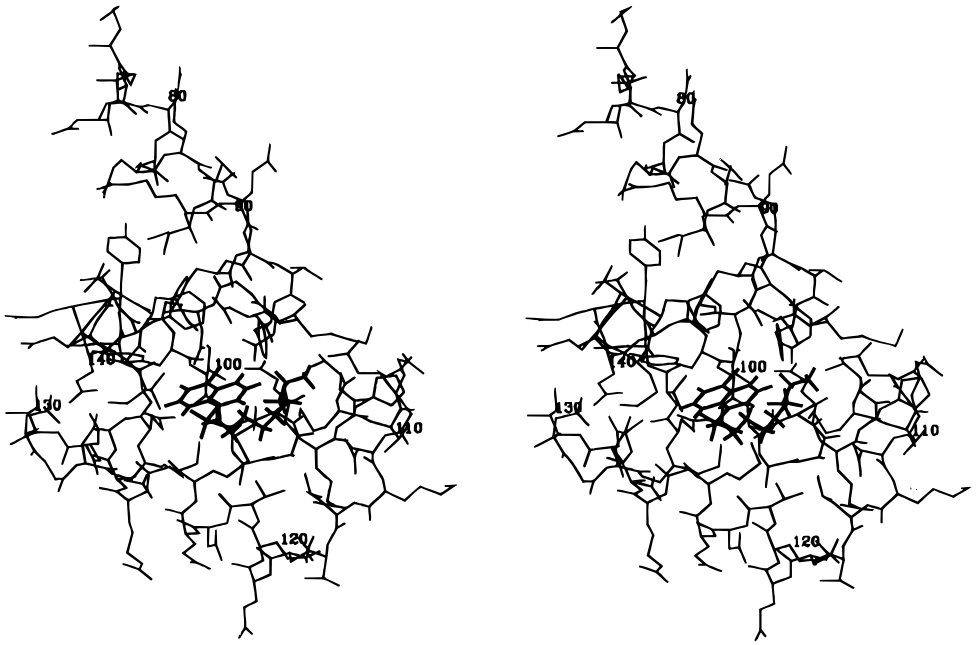

FIGURE 9: Heavy-atom wire-frame stereo image of the structure shown in Figure 8.

proximately rotated by 180° about the vector joining the iodine and sulfur atoms.

From the calculated set of structures, it was possible to analyze the constraints in order to find the dominating contribution(s) from the ambiguous constraint list and hence "assign" the cross-peaks. For the majority of constraints this was straightforward, as the same assignment was dominant in all structures (at least within the orientation class in which the constraint was satisfied), the only remaining ambiguity being between the pair of resonances M109 hb* and I100 hb. The chemical shifts of the resonances to which the cross-peaks were assigned are marked alongside the spectrum in Figure 6. These resonances include the majority of the residues lining the pocket (no NOEs could be identified to V136 as the methyl resonances are coincident with one of the drug resonances). These assignments were "checked" manually, by comparing the peaks with identified protein−protein peaks. Where possible, the reference peaks were in the same NOESY spectrum as was used for the structure calculations (or in the equivalent ^{15}N-selected spectrum). It was not possible to find a sufficiently unambiguous peak for some of the resonances, in which case peaks in the 3D TOCSY-HMQC or NOESY-HMQC spectra used for the protein assignment were used.

Similar calculations were then performed with randomized data in order to make an objective check that the dynamic assignment method was achieving correct, or at least substantially correct, assignments. If the method was making

a large number of incorrect assignments, then it should perform no better with the true experimental data than with randomized data. In the dynamic assignment method, the correct assignment of peaks and the calculation of the correct binding conformation are intimately related, since the correct assignment of peaks can only be achieved if the correct binding conformation is also calculated. Thus a comparison between experimental and randomized data sets can validate both the assignments and the calculated structure at the same time. Five randomized constraint data sets were constructed as described in Experimental Procedures, and 120 structures were calculated for each different data set. For these data sets, the calculations simply consisted of one cooling stage and one cycle of refinement. The NOE-equivalent distances for the constraints within this family of structures are plotted in Figure 7 (small symbols). The lowest energy structures for the calculations using the randomized constraints sets were consistently higher than those for the experimental data set, although the degree of convergence was rather similar (data not shown). In all cases (Figure 7, small symbols) the distances were also significantly longer than in the experimental data, the majority of constraints falling outside the shaded "allowed" region of the figure, thus confirming that the experimental data are substantially correctly assigned.

In order to gain more information about secondary binding events, a second filtered NOESY spectrum was also collected at an increased J-8•tr2c ratio of 1.6:1. The intensity of the stronger intermolecular cross-peaks in the 1:1 spectrum was effectively unchanged; however, a number of new intermolecular cross-peaks were observed. A filtered NOESY spectrum of the 2:1 J-8:CaM complex was also collected, which showed a very similar intensity of intermolecular cross-peaks as in the J-8:tr2c spectrum, although with additional peaks as expected for the two-domain case. Of particular note was the fact that the *t7*/*t8* NOE was still positive, as in the tr2c complex.

DISCUSSION

J-8 Binding to a Single Domain of CaM. In a complex such as this where the bound ligand retains a high degree of mobility, and where there is the possibility of the binding of secondary ligand molecules, the complex is not well described by the coordinates of an average structure in isolation but rather by a model combining structural, dynamical, and stoichiometric information. Such a description for the binding of J-8 to a single domain, tr2c, emerges from a combination of various pieces of experimental evidence. In this model, the evidence for which we discuss further below, tr2c binds one molecule of J-8 in the strongest (primary) binding event. This binding event involves the aromatic ring of J-8 binding into the hydrophobic pocket of tr2c, with the aliphatic tail extended into the solvent. The ring is relatively immobilized, and thus its rotational motion is indistinguishable from the overall correlation time of the protein. However, it can bind in one of two orientations, and within each orientation the ring retains some degree of translational freedom. In contrast, the aliphatic tail has a mobility similar to that of fully solvated basic residue side chains. There are also secondary binding event(s) with binding constants at least an order of magnitude smaller.

There are several pieces of experimental evidence that support the idea that the major interaction of J-8 with tr2c is via the aromatic ring and that the tail remains free. First, the sharpness of the *t7*/*t8* resonance in the COSY spectrum and the positive NOE between these two resonances indicate that the J-8 tail must be extremely mobile in the bound complex. In contrast, the intradrug aromatic−aromatic NOEs are of similar intensity to those of aromatic rings in the protein, which indicates that the aromatic ring is hindered in rotation. Finally, the largest shift changes in J-8 on binding are within the aromatic ring, while the shift changes in the tail are generally smaller (Table 1).

Full analysis of the chemical shift changes in tr2c upon J-8 binding is complex. In particular, the backbone shift changes appear to arise from a combination of various sources (see below), which precludes a direct analysis in terms of a particular J-8 binding site. Inspection of the chemical shift changes of the protein *side-chain* resonances on binding of J-8, however, reveals that the largest effects are seen in residues that form part of the hydrophobic pocket. The tr2c residues in Figure 8 are colored in blue tones according to the largest side-chain chemical shift change observed. The figure clearly shows that the majority of these residues affected by drug binding line the hydrophobic pocket, confirming the location of the binding site. A rear view of the molecule (not shown) is entirely free of color.

The fact that the exchange broadening is largely eliminated in the 1:1 solution (Figure 4) determines a stoichiometry of 1 for the primary binding event. A second characteristic of a single-site interaction is that the resonances in the $^{1}H/^{15}N$ HSQC spectrum will move in straight lines, regardless of the dependence of the proportion of bound protein on the ligand concentration. Evidence that a small but significant population of a secondary binding site must also exist in the 1:1 solution comes from the "anomalous" exchange broadening observed for resonances such as T110 and F89 (Figure 4) and the curvature of some of the traces in Figure 3a. The curvature arises when a resonance experiences shift changes due to both primary and secondary binding events. This will lead to either a distinct kink in the HSQC traces or a more gently curvature, depending on the difference in the affinities of the two sites. By chance, of course, a second interaction may shift the HSQC peak in the same direction as the first interaction. In this case, a much more definite indication of a second interaction is given if exchange broadening is observed for a peak. A corresponding variety of types of behavior is observed during the titration in this study (Figure 3a).

The resonance of T110 shows the greatest curvature in Figure 3a and is also strongly broadened such that it is only barely detectable in the 1:1 spectrum. This resonance is therefore strongly shifted by the secondary binding event. Several other resonances also show strong curvature, especially above the 1:1 point, in particular, M109 and M145 (see Figure 3b). These latter resonances do not, however, show a significant exchange broadening effect, so they must experience a comparatively small shift due to the secondary event. F89 is an example of a resonance which does not show curvature in Figure 3a but which drops to approximately 20% of initial intensity in the 1:1 spectrum. This resonance must therefore be shifted in the same direction by both interactions, the shift due to the second interaction being larger than that due to the first.

Owing to competitive binding arising from the second interaction, resonances such as F92 and F141 (which appear

to be shifted entirely by the first event) have not shifted to their full extent at the 1:1 point (Figure 3b). From this discrepancy, we estimate that the secondary binding site must be populated between 10% and 20% in a 1:1 solution. Using a simple model of binding where the secondary binding process has a stoichiometry of 1 and is independent of the primary event, this partitioning between the primary and secondary binding events would correspond to binding constants that differ by between 1 and 2 orders of magnitude. It is not clear from the distribution of affected residues that the binding of the second molecule is well localized or indeed whether it involves only a single drug molecule. The secondary binding may not be independent of the primary binding event, since it may involve an interaction with the primary binding molecule similar to the interactions observed between different TFP molecules in the recently reported crystal structure of a TFP·CaM complex (Vandonselaar *et al*., 1994). This would be consistent with the fact that the residues affected by the secondary event are all residues around the edge of the pocket. The ^{15}N-filtered NOESY spectrum of the 1.6:1 J-8·tr2c complex contains extra intermolecular cross-peaks which must correspond to secondary binding of one or more drug molecules, but these cross-peaks have not yet been assigned and further investigations are under way into the nature of the higher stoichiometry complexes of J-8 and tr2c. Our observation of secondary binding to the isolated C-terminal domain contrasts with the suggestion of Vandonselaar *et al*. that secondary TFP molecules only bind when CaM is in its globular form (as opposed to its more open, or dumbbell).

The evidence for translational mobility in the primary binding site comes from the weakness of the intermolecular NOEs observed. Even the strongest intermolecular NOEs were insufficiently intense to correspond to van der Waals contact. Since the exchange broadening is largely eliminated in the 1:1 solution, we know that each primary binding site is effectively fully occupied at the drug concentration at which the NOESY spectra were recorded, and from the binding constant we know that each drug molecule is predominantly in the bound form. The only explanation for the weakness of the intermolecular NOEs can therefore be that there is conformational heterogeneity within the bound form, leading to an averaging of the NOEs. We note that this weakness of NOEs is not necessarily a consequence of the system being in fast exchange, since the time scale of the fast exchange process ($\sim 10^{-3}$ s) is far larger than the time scale characteristic of positive NOEs ($\sim 10^{-9}$ s).

Finally, it is noteworthy that the methionine methyl resonance observed at 2.06 ppm in the free protein broadens significantly with the addition of the first 0.2 molar equiv of drug and does not fully resharpen in the 1:1 solution. Similar broadening of these resonances within intact CaM is observed on binding the drug calmidazolium (Reid *et al*., 1990). In the case of calmidazolium, the broadening was proposed to result from immobilization of the CaM methionine side chains due to the direct interaction of these residues with the drug. In light of the above results, there may also be a contribution to the broadening from secondary binding events as observed with J-8.

Effect of Introducing a Second Domain. When J-8 is titrated into intact CaM, the exchange broadening is largely eliminated in the 2:1 solution (*i.e*., not 1:1 solution as observed for J-8 plus tr2c), which establishes a stoichiometry of 2 for the primary binding event. This is not surprising since the tr1c domain of CaM contains a hydrophobic pocket equivalent to that of the tr2c domain. That one molecule binds to each domain is supported by the observation of shift changes in the C-terminal domain of CaM equivalent to those in tr2c described above and the similar range of magnitudes of shifts observed for the N-terminal domain. It appears that the binding affinities of the two domains are indistinguishable, since resonances in both domains moved by a similar amount during the addition of both equivalents of J-8.

The most surprising result, in the light of the generally accepted paradigm for a CaM antagonist, is that the mobility of the drug tail in the 2:1 J-8·CaM complex appears similar to that observed for the 1:1 J-8·tr2c complex. The line width of the *t7*/*t8* cross-peak and the differential with the *t1*/*t2* cross-peak in the COSY spectrum of the two complexes are very similar (Figure 5), and the NOE between *t7* and *t8* is positive in both complexes. The amine group thus appears to be fully solvated for each J-8 molecule: if one of the J-8 molecules in the 2:1 J-8·CaM complex were immobile, then owing to the rapid exchange relative to the relaxation time, its relaxation rate would dominate both the COSY and NOE observation. Therefore, there is no well-defined salt bridge formed between the amino group of J-8 and any individual carboxylate group of the protein. Indeed, if there is any interaction between the amine group of J-8 and any acidic residues on CaM, then it cannot be significantly restraining. The chemical shift changes observed in J-8 bound to CaM show the same pattern as when bound to tr2c, which is further evidence that the primary interaction remains that between the aromatic ring and the hydrophobic pocket.

There is a small difference between the J-8 off-rates as measured by NMR, the rate being slightly lower for the CaM system compared to tr2c. We cannot completely exclude the possibility of a small degree of cooperativity giving this difference by a factor of <5 in the off-rate. Alternatively, effects of this magnitude may simply reflect differences in the binding constant of the two domains (which we cannot determine to a high degree of accuracy), an electrostatic effect arising from the different charge state of the free and one-J8-molecule-bound forms of CaM, or the influence of the truncation of tr2c. The fact that the off-rates are of the same order of magnitude demonstrates that if there is any difference in the strength of interaction between the antagonist and the one- or two-domain proteins, then this effect can only be very small. This conclusion is confirmed by the fact that the intensities of the intermolecular NOEs are effectively unchanged, and so the bound conformation must retain much of the translational freedom observed for the one-domain system.

The interaction of J-8 with CaM thus appears to be that of the binding of two effectively independent molecules, one to each domain. The predominant interaction is simply between the aromatic ring of J-8 and the hydrophobic pockets of CaM. The amino tail of J-8 makes either no or only very weak interactions with the protein. In terms of the generally accepted paradigm for calmodulin antagonists, it is rather surprising that we find no direct role for the amino tail of the J-8 molecule. This feature may be required simply to boost the solubility of these rather insoluble compounds. It seems unlikely that such a binding mode should require or cause the CaM to form its globular form in solution, although

as we discuss below, this is something that it would be very difficult to prove by NMR.

TFP Binding. Our studies on TFP were prompted by the two recently published crystal structures of TFP·CaM (Vandonselaar *et al*., 1994; Cook *et al*., 1994). TFP is not such a ideal molecule for NMR studies as J-8, since the resonances from the piperazine ring are very broad in free TFP due to conformational exchange and are unobservable in the CaM·TFP complex. Thus in the tail we have only the resonances from the three methylenes and the *N*-methyl, which are inadequate to properly investigate the dynamics of the TFP tail. Furthermore, the chemical shift range of the aromatic resonances in TFP no longer allow the simple ^{15}N-filtering of the NOESY spectrum. However, we can still draw some important conclusions concerning the stoichiometry and general binding mode.

In the TFP titration, drug was added to a final ratio of 4:1, in order to investigate the stoichiometries seen in the X-ray structures. Again, resonances in both domains moved by similar amounts during the addition of the first 2 equiv of drug, with most of the exchange broadening eliminated at a ratio of 2:1. This implies that the primary binding event has a stoichiometry of 2. No evidence was seen for a saturated 1:1 complex in solution, as seen in the X-ray structure by Cook *et al*.

The amide and ^{15}N chemical shift changes observed on the addition of the first 2 equiv of drug are remarkably similar in magnitude and direction to those seen with J-8 (Figure 3a), which strongly suggests that the binding mode is very similar. Upon addition of a further 2 equiv of drug, additional smaller chemical shift changes were observed (Figure 3c), indicating that, under the crystallization conditions used by Vandonselaar *et al*. (35:1), multiple binding of TFP is likely to occur.

Sources of Chemical Shift Changes. A detailed interpretation of the chemical shift changes observed in these systems is complex. The most simple explanation would be that the shifts were due to a ring current effect from the aromatic ring of the drug, in which case one could readily determine the binding site. We have made theoretical calculations to see if this is plausible, based on the coordinates from the NMR study of the M13 peptide and *Drosophila* CaM (Ikura *et al*., 1992) using the chemical shift calculation program of Williamson *et al*. (1993). These calculations were unable to produce shifts of a magnitude and pattern similar to those observed. The large amide shifts observed for the aromatic residues F92 and F141 in fact suggest that many of the shifts are due to conformational changes in the aromatic residues of the protein itself.

If the shift changes were induced entirely by field effects (such as ring current fields of whatever source), then the proton and nitrogen shift changes should cover a similar range of magnitudes if expressed in parts per million. In fact, the nitrogen shifts are much larger than this, by a factor of approximately 5. The most likely reason for this is that the nitrogen shifts are largely induced by conformational changes in the protein backbone. One of the largest shifts that we observe is for residue T146 in the final helix of tr2c. This indicates that simply the binding of an aromatic ring into the hydrophobic pocket of tr2c can induce sufficient changes in the backbone structure to induce large nitrogen chemical shift changes. In the study of Ikura *et al*. (1991) relatively large shift changes were also observed in this region of CaM on binding the M13 peptide. The region in which they observed the greatest shift changes was in the central helix between residues 72 and 78, which was interpreted as evidence of a dramatic conformational change in the central helix, causing the molecule to form a compact globular structure. This is the region that contains the final helix of tr1c and hence is highly homologous to the final helix of tr2c. Since we now know from our studies that large shifts can be induced in tr2c in isolation, we believe that such shift changes cannot be used to provide unambiguous evidence of such a change in the structure of the central helix. In the case of the M13·CaM system the globular structure was later proven in an NOE-based structure determination; however, most of the constraints defining the globular structure in that study were derived from NOEs between the peptide and the protein. Unambiguously interpreting such NOEs where the peptide is replaced by *several* drug molecules would be extremely difficult. This question might be best answered by small angle scattering methods.

ACKNOWLEDGMENT

We thank Michael Nilges, Sheila MacNeil, Mike Williamson, Sture Forsén, Torbjorn Drakenberg, Bryan Finn, Johan Evenas, and Kay Sorimachi for helpful discussions.

SUPPORTING INFORMATION AVAILABLE

A table of the chemical shift changes in tr2c on binding J-8 (5 pages). Ordering information is given on any current masthead page.

REFERENCES

Andersson, A., Forsén, S., Thulin, E., & Vogel, H. J. (1983) Cadmium-113 nuclear magnetic resonance studies of proteolytic fragments of calmodulin: Assignment of strong and weak cation binding sites, *Biochemistry 22*, 2309−2313.

Andersson, A., Drakenberg, T., & Forsén, S. (1985) The interaction of various drugs with calmodulin as monitored by ^{113}Cd NMR, in *Calmodulin antagonists and cellular physiology* (Hidaka, H., & Hartshorne, D. J., Eds.) pp 27−44, Academic Press, Orlando, FL.

Andersson, S. R., & Malencik, D. A. (1986) in *Calcium cell function* (Cheung, W. Y., Ed.) Vol. 6, pp 1−42, Academic Press, London.

Babu, Y. S., Sack, J. S., Greenhough, T. J., Bugg, C. E., Means, A. R., & Cook, W. J. (1985) Three dimensional structure of calmodulin, *Nature 315*, 37−40.

Barbato, G., Ikura, M., Kay, L. E., Pastor, R. W., & Bax, A. (1992) Backbone dynamics of calmodulin studied by ^{15}N relaxation using inverse detected two-dimensional NMR spectroscopy: The central helix is flexible, *Biochemistry 31*, 5269−5278.

Bodenhausen, G., & Ruben, D. J. (1980) Natural abundance nitrogen-15 NMR by enhanced heteronuclear spectroscopy, *Chem. Phys. Lett. 69*, 185−189.

Brown, S. C., Weber, P. L., & Mueller, L. (1988) Towards complete H1 NMR spectra in proteins, *J. Magn. Reson. 77*, 166−169.

Brünger, A. T. (1992) *X-PLOR. A System for X-ray Crystallography and NMR*, Yale University Press, New Haven, CT.

Chattopadhyaya, R., Meador, W. E., Means, A. R., & Quiocho, F. A. (1992) Calmodulin structure refined at 1.7 Å resolution, *J. Mol. Biol. 228*, 1177−1192.

Cook, W. J., Leigh, J. W., & Walter, M. R. (1994) Drug binding by calmodulin: Crystal structure of a calmodulin-trifluoperazine complex, *Biochemistry 33*, 15259−15265.

Creighton, T. E. (1984) *Proteins: structures and molecular properties*, W. H. Freeman and Co., New York.

Dalgarno, D. C., Klevit, R. E., Levine, B. A., Williams, R. J. P., Dobrowolski, Z., & Drabikowski, W. (1984a) ^{1}H NMR studies

of calmodulin: Resonance assignments by use of tryptic fragments, *Eur. J. Biochem. 138*, 281−289.
Dalgarno, D. C., Klevit, R. E., Levine, B. A., Scott, G. M. M., Williams, R. J. P., Gergely, J., Grabarek, Z., Leavis, P. C., Grand, R. J. A., & Drabikowski, W. (1984b) The nature of the trifluoperazine binding sites on calmodulin and troponin-C, *Biochim. Biophys. Acta 791*, 164−172.
Finn, B. E., & Forsen, S. (1995) The evolving model of calmodulin structure, function and activation, *Structure 3*, 7−11.
Finn, B. E., Evenas, J., Drakenberg, T., Waltho, J. P., Thulin, E., & Forsén, S. (1995) Calcium induced structural changes and domain autonomy in Calmodulin, *Nat. Struct. Biol. 2*, 777−783.
Hait, W. N., & Lazo, J. S. (1986) Calmodulin: a potential target for cancer chemotherapeutic agents, *J. Clin. Oncol. 4*, 994−1012.
Hickie, R. A., Wei, J.-W., Blyth, L. M., & Wong, D. Y. W. (1983) Cations and calmodulin in normal and neoplastic growth regulation, *Can. J. Biochem. Cell Biol. 61*, 934−941.
Ikura, M., Kay, L. E., & Bax, A. (1990) A novel approach for sequential assignment of ^{1}H, ^{13}C, and ^{15}N spectra of larger proteins: Heteronuclear triple-resonance three-dimensional NMR spectroscopy. Application to calmodulin, *Biochemistry 19*, 4659−4668.
Ikura, M., Kay, L. E., Krinks, M., & Bax, A. (1991) Triple resonance multi-dimensional NMR study of CaM complexed with the binding domain of skeletal muscle myosin light-chain kinase: Indication of a conformational change in the central helix, *Biochemistry 30*, 5498−5504.
Ikura, M., Clore, G. M., Gronenborn, A. M., Zhu, G., Klee, C. B., & Bax, A. (1992) Solution structure of a calmodulin-target peptide complex by multidimensional NMR, *Science 256*, 632−638.
Lopes, M. C. F., Vale, M. G. P., & Carvalho, A. P. (1990) Ca^{2+}-dependent binding of tamoxifen to calmodulin isolated from bovine brain, *Cancer Res. 50*, 2573−2758.
MacNeil, S., Griffin, M., Cooke, A. M., Pettett, N. J., Dawson, R. A., Owen, R., & Blackburn, G. M. (1988) Calmodulin antagonists of improved potency and specificity for use in the study of calmodulin biochemistry, *Biochem. Pharmacol. 37*, 1717−1723.
Macura, S., Huang, Y., Suter, D., & Ernst, R. R. (1981) Two-dimensional chemical exchange and cross-relaxation spectroscopy of coupled nuclear spins, *J. Magn. Reson. 43*, 259−281.
Marion, D., Driscoll, P. C., Kay, L. E., Wingfield, P. T., Bax, A., Gronenborn, A. M., & Clore, G. M. (1989a) Overcoming the overlap problem in the assignment of ^{1}H NMR spectra of larger proteins by the use of three-dimensional heteronuclear ^{1}H-^{15}N Hartmann-Hahn multiple quantum coherence and nuclear Overhauser effect multiple quantum coherence spectroscopy: Application to interleukin-1-beta, *Biochemistry 28*, 6150−6156.
Marion, D., Ikura, M., & Bax, A. (1989b) Improved solvent suppression in one-dimensional and two-dimensional NMR spectra by convolution of time domain data, *J. Magn. Reson. 84*, 425−430.
McConnell, H. M. J. (1958) Reaction rates by nuclear magnetic resonance, *J. Chem. Phys. 28*, 430−431.
Meador, W. E., Means, A. R., & Quiocho, F. A. (1992) Target enzyme recognition by calmodulin: 2.4Å structure of a calmodulin-peptide complex, *Science 257*, 1251−1255.
Meador, W. E., Means, A. R., & Quiocho, F. A. (1993) Modulation of calmodulin: Plasticity in molecular recognition on the basis of X-ray structures, *Science 262*, 1718−1721.
Nicholls, A. (1993) *GRASP: Graphical Representation and Analysis of Surface Properties*, Columbia University, New York.
Nilges, M. (1993) A calculation strategy for the structure determination of symmetric dimers by ^{1}H NMR, *Proteins: Struct., Funct., Genet. 17*, 297−309.
Nilges, M. (1995) Calculation of protein structures with ambiguous distance restraints. Automated assignment of ambiguous NOE crosspeaks and disulphide connectivities, *J. Mol. Biol. 245*, 645−660.
Nilges, M., Clore, G. M., & Gronenborn, A. M. (1988a) Determination of three-dimensional structures of proteins from interproton distance data by hybrid distance geometry-dynamical simulated annealing calculations, *FEBS Lett. 229*, 317−324.
Nilges, M., Clore, G. M., & Gronenborn, A. M. (1988b) Determination of three-dimensional structures of proteins from interproton distance data by dynamical simulated annealing from a random array of atoms, *FEBS Lett. 239*, 129−136.
O'Neil, K. T., & DeGrado, W. F. (1990) How calmodulin binds its targets: Sequence independent recognition of amphiphilic α-helices, *Trends Biol. Sci. 15*, 59−64.
Otting, G., Senn, H., Wagner, G., & Wüthrich, K. (1986) Editing of 2D ^{1}H NMR spectra using X half-filters. Combined use with residue-selective ^{15}N labeling of proteins, *J. Magn. Reson. 70*, 500−505.
Prozialeck, W. C., & Weiss, B. (1982) Inhibition of calmodulin by phenothiazines and relayed drugs: structure-activity relationships, *J. Pharmacol. Exp. Ther. 222*, 509−516.
Rance, M., Sørensen, O. W., Bodenhausen, G., Wagner, G., Ernst, R. R., & Wüthrich, K. (1983) Improved spectral resolution in COSY ^{1}H NMR spectra of proteins via double quantum filtering, *Biochem. Biophys. Res. Commun. 117*, 479−485.
Rasmussen, C. D., Lu, K. P., Means, R. L., & Means, A. R. (1992) Calmodulin and cell cycle control, *J. Physiol. 86*, 83−88.
Reid, D. G., MacLachlan, L. K., Gajjar, K., Voyle, M., King, R. J., & England, P. J. (1990) A proton nuclear magnetic resonance molecular modelling study of calmidazolium (R24571) binding to calmodulin and skeletal muscle troponin C, *J. Biol. Chem. 265*, 9744−9753.
Sandström, J. (1982) *Dynamic NMR spectroscopy*, Academic Press, London.
Vandonselaar, M., Hickie, R. A., Quail, J. W., & Delbaere, L. T. J. (1994) Trifluoperazine-induced conformational change in Ca^{2+}-calmodulin, *Nat. Struct. Biol. 1*, 795−801.
Vogel, H. J., Lindahl, L., & Thulin, E. (1983) Calcium dependent hydrophobic interaction chromatography of calmodulin, tropinin C and their proteolytic fragments, *FEBS Lett. 157*, 241−246.
Waltho, J. P., & Cavanagh, J. (1993) Practical aspects of recording multidimensional NMR spectra in water with flat baselines, *J. Magn. Reson., Ser. A 103*, 338−348.
Wei, J.-W., & Hickie, R. A. (1981) Increased content of calmodulin in Morris hepatoma 5123 t.c. (h), *Biochem. Biophys. Res. Commun. 100*, 1562−1568.
Wei, J.-W., Morris, H. P., & Hickie, R. A. (1982) Positive correlation between calmodulin content and hepatoma growth rates, *Cancer Res. 42*, 2571−2574.
Williamson, M. P., & Asakura, T. (1993) Empirical comparisons of models for chemical-shift calculation in proteins, *J. Magn. Reson., Ser. B 101*, 63−71.
Wishart, D. S., Bigam, C. G., Yao, J., Abilgaard, F., Dyson, H. J., Oldfield, E., Markley, J. L., & Sykes, B. D. (1995) ^{1}H, ^{13}C and ^{15}N chemical shift referencing in biomolecular NMR, *J. Biomol. NMR 6*, 135−140.

BI9605043